THE ASTROPHYSICAL JOURNAL, 287:622–632, 1984 December 15

A MEASUREMENT OF THE ABSOLUTE FLUX OF COSMIC-RAY ELECTRONS

R. L. GOLDEN AND B. G. MAUGER[1]
New Mexico State University

AND

G. D. BADHWAR, R. R. DANIEL,[2] J. L. LACY, S. A. STEPHENS,[2] AND J. E. ZIPSE[3]
National Aeronautics and Space Administration, Johnson Space Center
Received 1983 September 6; accepted 1984 June 25

ABSTRACT

The absolute flux of cosmic-ray electrons has been measured using a balloon-borne superconducting magnet spectrometer. The instrument consisted of a gas Cerenkov detector, a momentum spectrometer, and a lead-scintillator shower counter. The flux of electrons in the interstellar medium was determined by correcting the observed flux for energy loss in the atmosphere and the payload and for solar modulation. The flight was made at an average atmospheric depth of 5.8 g cm^{-2}, and the solar modulation was taken to be 300 MeV. The flux in the interstellar medium was found to be $367E^{-(3.15\pm0.2)}$ e^- m^{-2} sr^{-1} s^{-1} GeV^{-1} in the energy interval 4.5–63.5 GeV. The uncertainty in the absolute flux is 10%. The result has been validated by the use of data from a second balloon flight, the use of alternate selection criteria, and simultaneous measurement of other absolute fluxes.

Subject headings: cosmic rays: abundances — cosmic rays: general

I. INTRODUCTION

The electron is the lowest-mass constituent of the cosmic rays. In contrast to heavier cosmic rays, acceleration and propagation processes for electrons are affected by synchrotron energy loss and inverse Compton scattering. Consequently, electron flux observations can be compared with other cosmic-ray measurements (often with the use of radio measurements as additional information) to yield insight into cosmic-ray acceleration and propagation processes.

A very large number of experiments have been carried out to determine the electron energy spectrum. However, there is significant variation (about a factor of 4) in the absolute fluxes. This inconsistency in the observations gives rise to the suspicion that the higher flux observations may be contaminated with protons, thus obscuring the information unique to electron fluxes. Particular care has been taken in this experiment to determine the absolute e^- flux. Unlike previous experiments, this observation includes simultaneous measurement of other fluxes, and includes redundant methods for recognizing e^-. It should be noted that most previous experiments did not distinguish between e^+ and e^-. Consequently, the absolute rates reported here must be multiplied by ~ 1.1 for comparison with experiments that observed the combined e^+ and e^- fluxes. The e^+ flux is reported to be ~ 0.1 of the e^- flux (for example, see Buffington, Orth, and Smoot 1975). A separate publication is being prepared to report e^+ observations related to the e^- fluxes described here.

In this paper the units of rigidity (momentum/charge) or its inverse (called magnetic deflection) are used when referring to particles at the payload, and units of energy are used when referring to particles in the interstellar medium. Energies and fluxes are corrected to the interstellar medium, taking into account solar modulation and bremsstrahlung energy losses. The method used is described in detail elsewhere (Mauger 1981).

II. THE APPARATUS

The magnet spectrometer shown in Figure 1 has been described previously (Golden *et al.* 1978). It consisted of (*a*) a gas Cerenkov detector (G) having a threshold Lorentz factor of 40; (*b*) scintillators S1 and S2 for charge estimation; (*c*) eight multiwire proportional counters (MWPC) with spatial resolution of 220 μm on the axis where the deflection due to the magnetic field was greatest; and (*d*) seven scintillators (P1–P7), each separated by 1.2 radiation lengths of lead. Signals from all scintillators and from G were pulse-height analyzed.

The MWPCs utilize the distributed delay-line technique described in Lacy and Lindsey (1974). Each MWPC delivers two time values. The sum of these values should equal the total delay of the delay line. The difference of the delay times yields the position of a particle as it passed through the chamber. The time sum acts as a reliable check on data validity for a particular MWPC. In this paper a "good" MWPC measurement is defined as one in which the time sum had the expected value. The magnet was operated at a current of 120 A, producing a magnetic field of 10–40 kilogauss in the MWPC region. The measured resolution of the instrument corresponds to a maximum detectable rigidity of 80 GV/*c*. Events satisfying the trigger criterion of S1 · P1 · P7 were accepted for analysis. The geometric factor for this trigger is 324 ± 5 cm^2 sr^{-1}. The data reported here were obtained during a balloon flight from Palestine, Texas, in May 1976 under 5.8 g cm^{-2} of residual atmosphere. The total exposure time was 6.81×10^4 s. The instrument live-time fraction was 0.80. During the flight a total of 0.16 radiation lengths of material was in the atmosphere above the payload, and 0.08 radiation lengths of material was in the payload above the momentum spectrometer.

[1] Present address: NASA/Goddard Space Center, Greenbelt, MD.
[2] Present address: Tata Institute for Fundamental Studies, Bombay, India.
[3] Present address: Jet Propulsion Laboratory, Pasadena, CA.

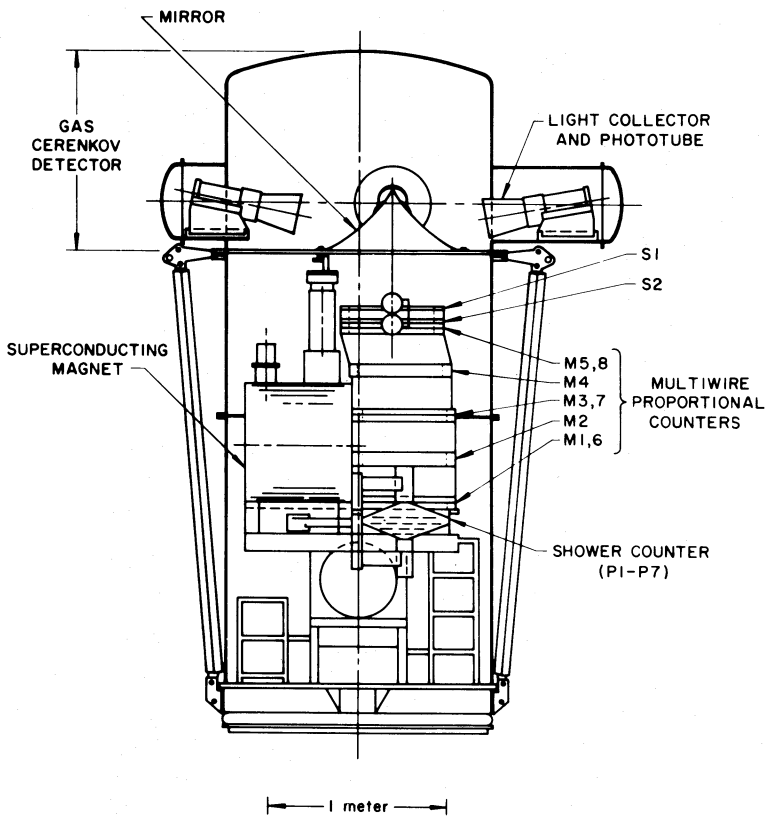

FIG. 1.—The experimental apparatus. S1 and S2 are charge-measuring scintillators, M1–M8 are the multiwire proportional counters, and P1–P7 are the shower-counter scintillators.

III. DATA ANALYSIS

All particles which satisfied the initial trigger criterion of S1 · P1 · P7 were recorded for later analysis. The basic strategy in the subsequent analysis was to look for particles with a negative charge (as deduced from the curvature in the magnetic field) which had at least a small interaction in the shower counter. The second criterion is necessary to eliminate μ^- mesons created by interactions in the atmosphere above the payload. This criterion also helps reduce proton (p) and antiproton ($\bar{p}$) backgrounds. In quantitative terms the selection criteria were the following:

1. At least five x-axis (axis of bending) and three y-axis (axis parallel to the magnetic field) MWPC readouts must have good time sums. In addition, the bottom pair of MWPCs must both have good time sums, the trajectory must give a least squares fit with $\chi^2 < 50$ on the x-axis and $\chi^2 < 30$ on the y-axis, and finally the curvature must correspond to a negative charge. The χ^2 criteria were derived from ground and accelerator testing.

2. The pulse height in S1 and S2 must correspond to a charge $Z \leq 1.8I_0$. I_0 is the pulse height of a singly charged relativistic particle.

3. The sum of the pulse heights in counters P1–P7 correspond to at least $50I_0$. This criterion corresponds to one-fourth the shower size typically associated with a 5 GV electron.

It is expected that electrons of 3 GV or greater energy would meet the above criteria with nearly 100% efficiency. However, there are other particles which could also meet the criteria. They include protons with misidentified curvature (called spillover protons), $\bar{p}$ from the galactic cosmic rays or produced in the atmosphere, π^- produced in the atmosphere, and of course e^- produced in the atmosphere. Atmospherically produced e^- cannot be distinguished from galactic e^-, but fortunately their contribution to the observed flux is expected to be small. The expected secondary e^- flux is calculated using fluxes given by Stephens (1981) and is subtracted from the observed flux. The correction is $\sim 10\%$ at low energies and decreases to a few percent at high energies.

Note that the remaining "contamination" is due to strong interacting particles (hadrons) with much more mass than the electron. Additional selection criteria based on shower-counter and Cerenkov counter responses can thus be used to decrease and/or measure the contamination.

Before imposing additional selection criteria, it is worth summarizing the amount of expected contamination. The spillover proton contamination is dominant at the highest energies. A proton with rigidity of 80 GV is only 2 σ from appearing to be a negatively charged particle with a rigidity of 80 GV. Since the proton flux is ~ 100 times the electron flux, we may expect the events selected by our initial criteria to be mostly spillover protons at the highest energies. Galactic and atmospheric $\bar{p}$ fluxes should be present at all energies, and they should comprise $\sim 13\%$ of the e^- flux (Golden *et al.* 1979*a*). The requirement that there be an interaction in the shower counter reduces the expected $\bar{p}$ content to $\sim 4\%$ of the sample. The π^- content has been calculated to be $\sim 5\%$ of the e^- flux (Stephens 1981). The requirement of a shower-counter interaction reduces the expected π^- contamination to less than 2%. The objective of additional tests and selection criteria is to measure and/or remove these sources of contamination.

The G-counter provides a clear-cut test for heavier particles

in the electron candidate sample. The efficiency of the G-counter was measured prior to the flight to be 0.66 for fully relativistic sea-level muons (Golden *et al.* 1978). If the electron candidate sample is all electrons, the G-on flux should be 0.66 of the total electron candidate sample. If there is a significant contamination of protons and antiprotons, the G-on flux will be less than 0.66 of the total. The pion Cerenkov threshold is about 6 GV. Thus pions below 6 GV would also contribute to the total sample but not to the G-on subset. Figure 2 shows the magnetic deflection distribution of the total electron candidate sample and the G-on subset. The points from the total sample have been multiplied by 0.66 for direct comparison. Both curves appear as one might expect for an incident spectrum which is a power law in rigidity modified by the geomagnetic cutoff and broadened by the bremsstrahlung energy losses. In the deflection region from -0.2 to -0.1 c/GV, the slight excess of the total sample above the G-on sample is consistent with that expected due to $\bar{p}$. The total sample shows an increasing excess from -0.1 c/GV toward 0.0 c/GV, indicating an increasing fraction of spillover protons.

The imposition of the G-on requirements should greatly reduce the heavy-particle content. Figure 2 shows that use of the G-on criterion produces the expected results. Consequently this criterion has been imposed for the final data set.

Another possible method for distinguishing background particles is based on determining the starting point for the shower-counter interactions. Incident electrons must initiate an electromagnetic cascade starting very near the top of the shower counter. The background particles (other than atmospheric e^-) must have undergone a nuclear interaction in the shower counter in order to have been selected as electron candidates (these particles are all hadrons). Since the shower counter is about one-third of a nuclear mean free path thick, the distribution of starting points for these particles should be flat, except for a small bias toward early interactions, introduced by the requirement of a minimum shower size.

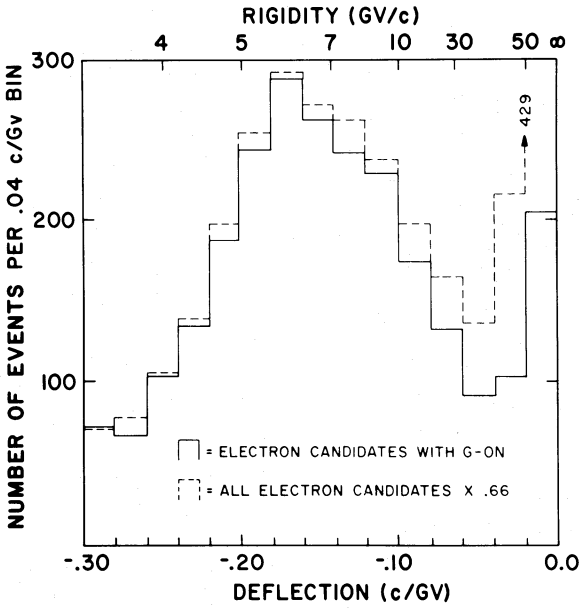

FIG. 2.—Deflection distribution of electron candidates. The rise at the right is believed to be proton background. The mean geomagnetic cutoff was at a deflection of 0.22 c/GV. The cutoff is broadened by bremsstrahlung energy losses in the atmosphere above the payload.

The shower starting points have been calculated by fitting the P1–P7 pulse heights to the hypothesis that the shower was an electromagnetic cascade. The starting point and total energy of the cascade were free parameters in the fit. For purposes of comparison, a sample of protons was also subjected to this same fitting process. The protons were obtained by the electron selection criteria, except for requiring that G be off and the curvature be positive. Figure 3 shows the results of this fitting process for various rigidity intervals. Figures 3*a*–3*d* show the electron candidate data with the additional requirement that G be on, and Figures 3*e*–3*h* are the corresponding proton distributions. Figure 3*a* shows the distribution of starting points one might expect for a pure electron sample. It contrasts sharply with the broad distribution for protons, shown in Figure 3*e*. We conclude that in the rigidity interval 3.33–25.0 GV there are very few background events in the G-on electron candidate sample. In the higher energy intervals (Figs. 3*c* and 3*d*) one can observe increasing numbers of early and late showers, indicating an increasing background in the electron candidate sample. In the highest rigidity interval the background has increased to the point where the electron flux is no longer distinguishable. The background is believed to be spillover protons.

In order to study the starting-point distribution quantitatively, the data were divided into rigidity intervals, and the electron candidate starting-point distributions were compared with starting-point distributions of the protons having the corresponding positive rigidity.

In any particular rigidity interval, the presence of early or late starting points is regarded as an indicator that hadrons are present in the sample of electron candidates. The proton sample from the corresponding positive rigidity interval is used to determine the ratio of the total number of hadron showers to (early + late) hadron showers. This ratio is called M, the background multiplier. The background in an e^- sample is then estimated as M times the number of (early + late) showers in the sample.

Electron starting-point distributions have been studied at the Stanford Linear Accelerator using 5–14 GeV electron beams. The shower starting points are measured (fitted) in radiation lengths relative to the first scintillator. Starting points above the first scintillator are regarded as positive, and those below the first scintillator are regarded as negative. The observed distributions peaked at $\sim +0.7x_0$. This is an artifact of the computer program, which had a small offset in the radiation-length coordinate. The width of this peak was $\sim \pm 1x_0$. Virtually no electrons were found with starting points outside the interval $+3.5x_0$ to $-2.5x_0$. Early and late showers are thus defined to be showers with starting points outside this interval. They are all presumed to be due to the hadron background.

With these criteria we find that values of M are typically ~ 4. This means that each early or late shower corresponds to ~ 4 hadrons in the electron candidate sample. Table 1 shows the detailed results of the starting-point analysis. The following formulas were used to calculate the number of electrons in a particular rigidity interval.

$$N_e = N_{\text{G-on}} - M_{\text{SP}} N_{\text{EL}} - N_{\text{SE}} ,$$

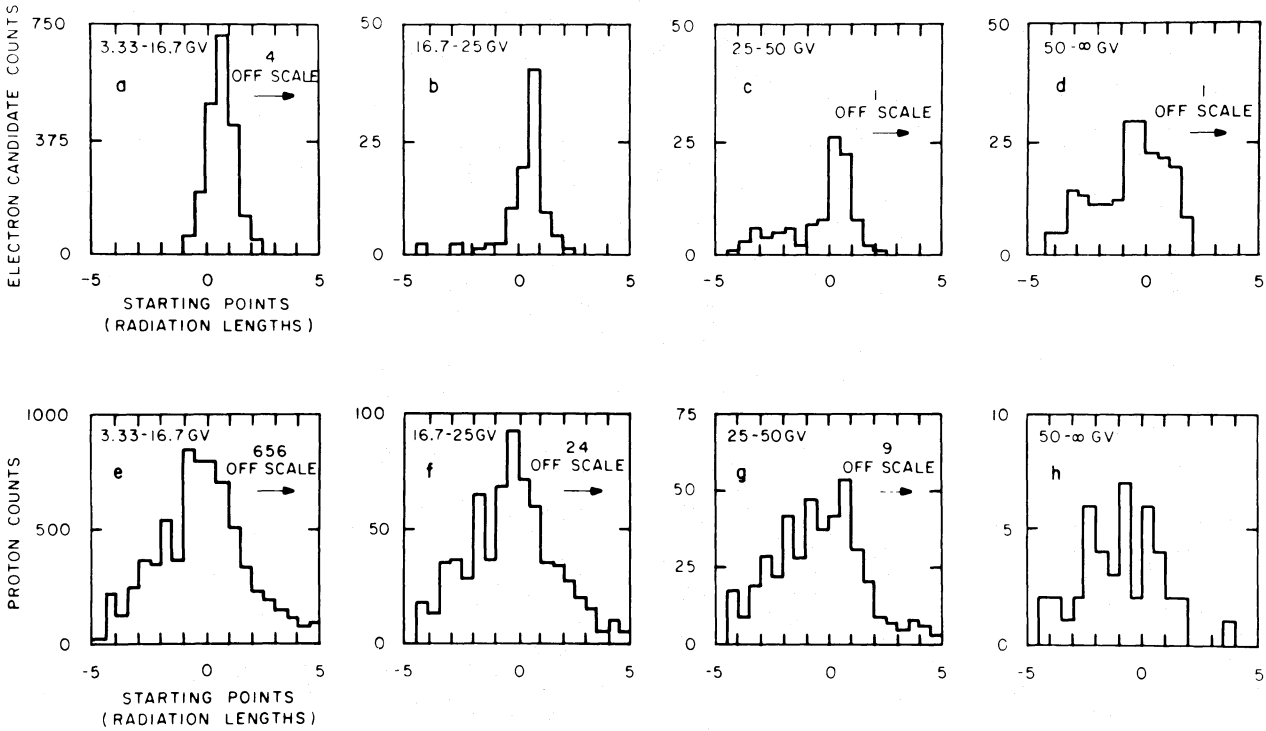

FIG. 3.—Shower starting points for electron candidates and protons. Positive starting points are above the first scintillator. For electrons, the starting-point distribution is expected to peak near the top of the shower counter (see Fig. 3*a*). For protons, the distribution is very broad (see Fig. 3*c*). It shows a peak because the requirement on minimum cascade size biases the selection process toward protons that interact early.

TABLE 1

SUMMARY OF ELECTRON OBSERVATIONS AND BACKGROUNDS

ρ (1)	$N_{\text{G-on}}$ (2)	N_{SE} (3)	N_{EL} (4)	M_{SP} (5)	$(N_e)_{\text{SP}}$ (6)	N_{SS} (7)	M_{SS} (8)	$(N_e)_{\text{SS}}$ (9)
3.33–3.57	73	8	0	4.93 ± 1.14	65 ± 9	23	1.16 ± 0.09	38 ± 7
3.57–3.85	68	7	0	4.93 ± 1.14	61 ± 8	13	1.14 ± 0.06	46 ± 7
3.85–4.17	104	7	1	4.37 ± 0.74	93 ± 10	13	1.09 ± 0.03	83 ± 10
4.17–4.56	134	6	0	3.83 ± 0.41	128 ± 12	12	1.11 ± 0.03	115 ± 11
4.56–5.00	189	6	0	3.84 ± 0.29	183 ± 14	14	1.12 ± 0.02	167 ± 13
5.00–5.56	244	5	1	3.91 ± 0.23	235 ± 16	18	1.16 ± 0.02	218 ± 15
5.56–6.25	289	5	0	3.86 ± 0.19	284 ± 17	7	1.19 ± 0.02	276 ± 17
6.25–7.14	263	5	1	3.59 ± 0.16	254 ± 16	11	1.26 ± 0.02	244 ± 16
7.14–8.33	242	4	1	3.94 ± 0.19	234 ± 16	5	1.35 ± 0.03	231 ± 15
8.33–10.00	230	3	0	4.40 ± 0.23	227 ± 15	2	1.43 ± 0.03	224 ± 15
10.00–12.50	175	3	1	4.11 ± 0.22	168 ± 14	3	1.68 ± 0.05	167 ± 13
12.50–16.67	132	2	2	4.88 ± 0.32	120 ± 13	8	1.68 ± 0.05	117 ± 11
16.67–25.00	92	2	4	5.00 ± 0.35	70 ± 12	8	2.05 ± 0.08	74 ± 10
25.00–50.00	103	1	16	4.44 ± 0.31	31 ± 18	24	2.21 ± 0.12	49 ± 10
50.00–∞	204	1	41	5.10 ± 1.44	-6 ± 30	56	2.90 ± 0.30	41 ± 24

Col. (1).—Rigidity at payload (GV/*c*).
Col. (2).—Number of G-on candidates.
Col. (3).—Secondary electrons.
Col. (4).—Number of early or late showers.
Col. (5).—Background multiplier for early or late showers.
Col. (6).—Number of e^- as determined by the starting-point technique.
Col. (7).—Number of electron candidates with shower sum $< 150 I_0$.
Col. (8).—Background multiplier for small shower-sum events.
Col. (9).—Number of e^- as determined by the shower-sum technique.

where

$N_{G\text{-on}}$ = number of G-on electron candidates;
M_{SP} = starting-point distribution background multiplier, which equals (number of protons) divided by (number of protons with early or late shower) for the proton sample;
N_{EL} = number of G-on electron candidates with early or late showers;
N_{SE} = estimated number of atmospheric secondary electrons.

Assuming that $(N_{G\text{-on}} - N_{EL})$ and N_{EL} are statistically independent quantities, the uncertainty in N_e is

$$\Delta N_e = [(N_{G\text{-on}} - N_{EL}) + (1 - M_{SP})^2 N_{EL} + N_{EL}{}^2 \Delta M_{SP}{}^2 + N_{SE}]^{1/2} .$$

Table 1 clearly shows that for rigidities of less than 12.5 GV, the hadron background in the G-on electron candidate sample is very low (less than 1%). Thus the absolute fluxes reported here are based on data that were gathered virtually without hadron background below 12.5 GV. Above 12.5 GV the background increases, owing to the increasing probability of spill-over protons satisfying the selection criteria. Note also that the uncertainty in the background multiplier also increases at higher energies. This adds to the difficulty of performing the background subtraction, and is due to declining statistics in the proton sample.

Electron-proton discrimination can also be done by using shower size rather than starting point. Studies of the shower-counter response to 5–14 GeV electrons made at the Stanford Linear Accelerator show that the sum of pulse heights P1–P7 is given roughly by $(100 + 20E)I_0$, where E is the electron energy. The mean shower sum for a proton with an interaction in the shower counter is almost constant at $\sim 100I_0$. Thus at higher energies the shower sum becomes a viable indicator for electron-proton discrimination. Figures 4*a*–4*d* show the shower-sum distributions for the electron candidates, and Figures 4*e*–4*h* show the corresponding distribution for protons. In the lowest energy interval, the electron candidates show a peak at $\sim 200I_0$ with few or no events lost due to the minimum shower sum required ($50I_0$). In contrast, the proton distribution is strongly peaked at the minimum shower sum. The complete absence in Figure 4*a* of a peak at the lowest shower sum is again clear evidence that the G-on electron candidates do not contain significant hadron contamination at the lower energies. At higher energies (Figs. 4*b*–4*d*) one can observe both the increasing hadron contamination (as a peak at the lowest pulse heights) and the increasing average pulse height of the electron showers. Note that even at the highest energies there is an apparent difference in the distribution for the electron candidates (Fig. 4*d*) and the corresponding proton distribution (Fig. 4*h*).

The shower sums have been analyzed by a method similar to the starting-point analysis. In this analysis, particles with shower sums less than $150I_0$ were regarded as hadron background. The background multiplier was determined for each rigidity interval as the ratio of the total number of protons to

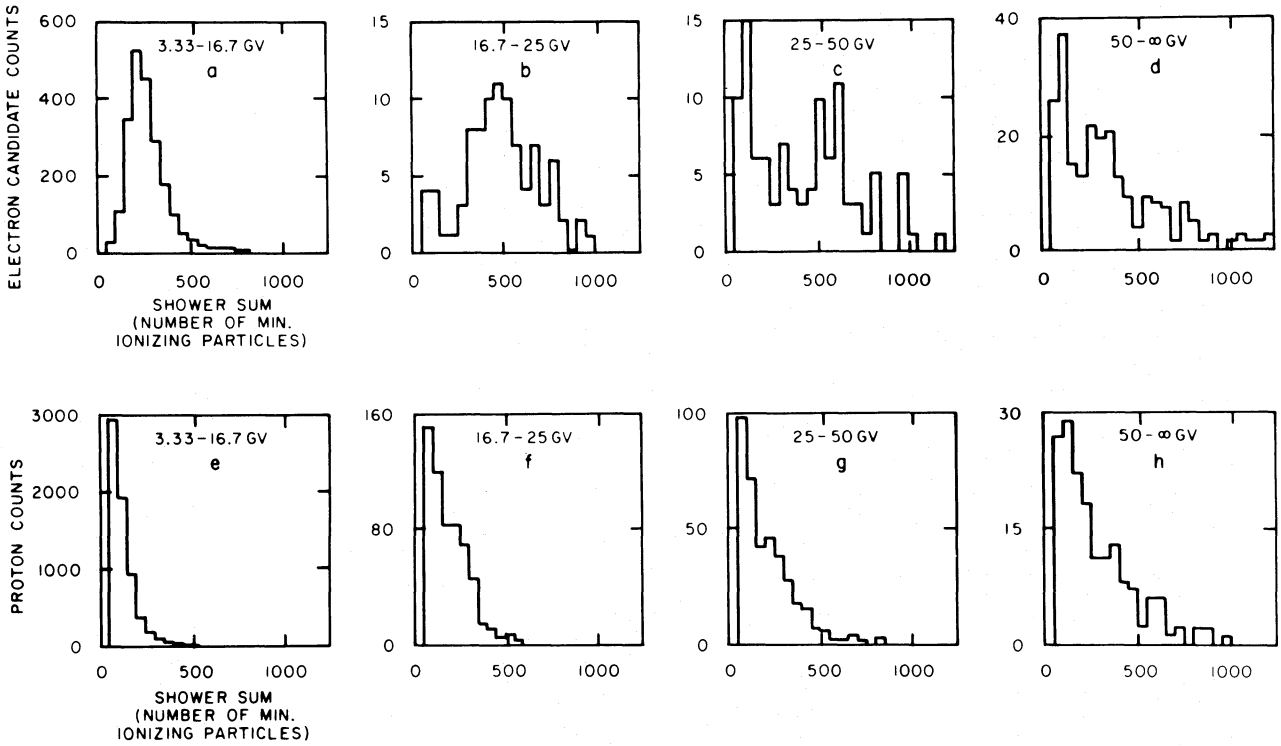

FIG. 4.—Shower-sum distributions for electron candidates and protons. Figure 4*a* is plotted using electron candidate data. It shows a broad peak corresponding to the mean shower sum expected for electrons in the 3.33–16 GV rigidity range. As the rigidity increases, the mean value of the shower sum should also increase. Figure 4*e* is plotted using events selected with G off and positive curvature. This sample is expected to be mostly protons. The peak at low pulse height is to be expected because of the relatively low multiplicity normally associated with proton collisions. The differences between Figs. 4*a* and 4*e* clearly illustrate the lack of proton contamination in the electron candidates at rigidities < 16 GV/*c*. At higher energies the similarity between the proton distributions and the electron candidate distributions are suggestive of increasing proton contamination in the electron sample. This is quite consistent with the conclusions drawn from Fig. 3.

the number of protons with shower sums less than $150I_0$. The electron flux was calculated from

$$N_e = N_{\text{G-on}} - M_{\text{SS}} N_{\text{SS}} - N_{\text{SE}} ,$$

where N_{SS} is the number of electron candidates with shower sum less than $150I_0$, and M_{SS} is the background multiplier for the shower-sum technique. The requirement of a minimum shower sum of $150I_0$ can be expected to cause N_e to be incorrect at low energies, owing to loss of real electrons. However, at higher energies ($\gtrsim 8$ GeV) very few, if any, electrons should be lost. In this technique, the background multiplier, M_{SS}, has the value of ~ 1. Since it is much smaller than for the starting-point analysis, one can expect the effect of uncertainties in M to have less impact on the uncertainties in N_e.

Table 1 also shows the results of the shower-sum analysis. As expected, the values of N_e at low energies are smaller than those derived from the starting-point distribution. Note that at rigidities above ~ 8 GV, the two techniques give consistent results. However, at higher energies, the smaller values of M and ΔM for the shower-sum method allow better separation (i.e., smaller values of ΔN_e) than the starting-point distribution.

In subsequent analyses we will use N_e determined by the starting-point method for rigidities up to 16.67 GV, and for rigidities above 16.67 GV we will use N_e determined by the shower-sum method.

The selection efficiencies for electron events are summarized in Table 2. The initial selection criterion was the occurrence of pulses > 50 mV in detectors S1, P1, and P7 within a 100 μs time interval. Pulse heights in all three counters were continuously monitored to ensure that gain changes or discriminator threshold changes did not occur during the flight. This initial selection criterion is assumed to have 100% efficiency. The geometric factor for this trigger was verified by extrapolation of the recorded trajectories to the horizontal plane of each detector. All detectors were fully "illuminated" by cosmic-ray triggers throughout the flight.

The experiment data acquisition system takes only ~ 40 μs to digitize an event. Since the rate of triggers was 1 per 20 ms, the apparatus is essentially without dead time. However, events are lost because of the limited telemetry rate. Events that are recognized by the flight apparatus but not transmitted to the ground are counted in an on-board scalar. The live-time efficiency is the ratio of events transmitted to total events recognized. This efficiency was cross-checked using the observed transmission rate and a mathematical model of the on-board buffering and transmission system.

The efficiency of the MWPC selection criteria was determined both before and during the flight. Singly ionizing particles were selected by imposing separate single-charge selection criteria on S1, S2, and P1–P7. The efficiency of the MWPC selection criteria was taken to be the fraction of these carefully chosen singly charged particles that passed the MWPC selection criteria. This technique yields the same efficiencies on the ground, using sea-level muons, and in flight (where the events are predominantly protons). This technique has also been validated at the Stanford Linear Accelerator. The repeatability of the efficiency measurements has been estimated by using reasonable variations in selection criteria, repeatability measurements over long-term intervals, and intercomparison of flight and ground measurement data. It was found to be $\Delta\epsilon/\epsilon \approx 0.08$.

TABLE 2

ELECTRON SELECTION EFFICIENCIES

Selection Factor	Efficiency
Scintillators, $Z < 1.8$	0.97
Live time	0.80
Multiwire proportional counters	0.58
Cerenkov detector	0.66
Shower detector	1.00
Overall efficiency[a]	0.30

[a] The overall efficiency shown does not include corrections for losses due to upward-moving particles from the shower counter during cascades. This additional correction is discussed in the text.

The efficiency corresponding to the S1, S2 pulse-height selection was determined by selecting events with all MWPCs good and P1–P7 showing a singly ionized particle. The efficiency was found to be 0.97 before, during, and after the flight.

The G-counter efficiency was determined prior to flight, using momentum spectrometer information to select μ mesons well above the Cerenkov threshold. The efficiency was found to be 0.66 for fully relativistic μ mesons.

In addition to the above efficiencies, studies of the instrument (with magnet on) at the Stanford Linear Accelerator show that electrons have an additional efficiency correction as a result of albedo (backward-traveling) particles generated by the electromagnetic cascades. The albedo particles provide an additional failure mode of the good time-sum tests beyond the efficiency already mentioned for singly ionized particles. This additional efficiency factor was measured from $\rho = 5$ GV/c to $\rho = 14$ GV/c and was found to be of the form

$$\epsilon = (1 - 0.044 \ln \rho) .$$

IV. RESULTS

Table 3 summarizes the electron fluxes observed at the payload. The number of electrons in each rigidity interval, N_e, is derived from Table 1 using the starting-point method below 16.67 GV and using the shower-sum method above 16.67 GV. The exposure factor, $A\Omega\tau\epsilon$, has an overall uncertainty factor of $\sim 10\%$. This uncertainty is not included in the columns for fluxes J_p and J_G. The mean energies, $\bar{E}_p$, and effective energy intervals, ΔE_p, are determined by appropriate convolutions with the assumed power-law spectrum (e.g., see Buffington, Orth, and Smoot 1975). The flux of e^- observed at the payload is $J_p = N_e/(A\Omega\tau\epsilon\Delta E_p)$.

The flux at the payload differs from the flux in the local interstellar medium (ISM) because of solar modulation, geomagnetic cutoff, and bremsstrahlung energy losses in the payload and in the atmosphere above the payload. The bremsstrahlung losses are difficult to account for. The mean energy loss is readily calculable, but often an electron can lose far more than the average amount of energy. This results in a substantial smearing of the energy distribution and causes a number of electrons to be observed well below the geomagnetic cutoff. In order to account for the large statistical fluctuation in bremsstrahlung losses, a Monte Carlo program was devised that would calculate absolute fluxes of e^- in the payload, given an absolute spectrum of e^- in the local ISM (Mauger 1981). We have used this program to transform the balloon altitude fluxes into galactic fluxes for comparison to other observations. This transformation was accomplished as follows: if the bremsstrahlung losses are treated as average energy losses (i.e., statistical fluctuations are ignored), each rigidity interval in the

TABLE 3

SUMMARY OF ELECTRON FLUX COMPUTATIONS

ρ (1)	N_e (2)	$A\Omega\tau\epsilon$ (3)	$\bar{E}_p$ (4)	ΔE_p (5)	J_p (6)	$\bar{E}_G$ (7)	ΔE_G (8)	ϵ_p (9)	J_G (10)
3.33–3.57	65 ± 9	641	3.45	0.24	0.42 ± 0.06	4.68	0.30	0.10	3.50 ± 1.56
3.57–3.85	61 ± 8	619	3.70	0.27	0.37 ± 0.05	5.01	0.35	0.13	2.17 ± 0.58
3.85–4.17	93 ± 10	619	4.00	0.32	0.47 ± 0.05	5.39	0.41	0.21	1.77 ± 0.28
4.17–4.56	128 ± 12	619	4.35	0.38	0.54 ± 0.05	5.83	0.48	0.33	1.33 ± 0.16
4.56–5.00	183 ± 14	619	4.76	0.45	0.66 ± 0.05	6.35	0.58	0.51	1.00 ± 0.10
5.00–5.56	235 ± 16	619	5.26	0.55	0.69 ± 0.05	6.99	0.70	0.70	0.76 ± 0.07
5.56–6.25	284 ± 17	619	5.88	0.69	0.67 ± 0.04	7.78	0.88	0.85	0.62 ± 0.05
6.25–7.14	254 ± 16	619	6.66	0.89	0.46 ± 0.03	8.77	1.13	1.00	0.36 ± 0.03
7.14–8.33	234 ± 16	597	7.69	1.18	0.33 ± 0.02	10.08	1.50	1.03	0.25 ± 0.02
8.33–10.00	227 ± 15	597	9.09	1.65	0.23 ± 0.02	11.85	2.10	1.06	0.17 ± 0.01
10.00–12.50	168 ± 14	597	11.10	2.46	0.11 ± 0.01	14.42	3.14	1.10	0.082 ± 0.008
12.50–16.67	120 ± 13	575	14.27	4.07	0.051 ± 0.006	18.45	5.18	1.14	0.035 ± 0.004
16.67–25.00	74 ± 10	575	19.95	7.94	0.016 ± 0.002	25.69	10.13	1.12	0.011 ± 0.002
25.00–50.00	49 ± 10	553	33.08	21.79	0.41 ± 0.08(−2)	42.47	27.89	1.23	0.26 ± 0.05(−2)
50.00–∞	41 ± 24	530	91.67	158.10	0.49 ± 0.29(−3)	119.40	213.20	2.69	0.14 ± 0.08(−3)

Col. (1).—Rigidity at payload (GV/*c*).
Col. (2).—Number of electrons.
Col. (3).—Exposure factor.
Col. (4).—Effective mean energy at payload (GeV).
Col. (5).—Effective energy interval at payload (GeV).
Col. (6).—Flux at payload (electrons m^{-2} sr^{-1} s^{-1} GeV^{-1}).
Col. (7).—Effective mean energy in Galaxy.
Col. (8).—Effective energy interval in Galaxy (GeV).
Col. (9).—Propagation efficiency.
Col. (10).—Flux in Galaxy (electrons m^{-2} sr^{-1} s^{-1}).

payload transforms into an energy interval in galactic space. The corresponding intervals are noted in Table 3. In order to correct for energy spreading due to statistical fluctuations in energy loss, we have used the Monte Carlo energy-loss program to determine a propagation efficiency, ϵ_p, for each of the energy intervals. This efficiency represents the coupling constant between each galactic energy interval and its corresponding payload interval. It also incorporates the geomagnetic cutoff effects. Previous authors have corrected for average energy losses and geomagnetic effects but did not correct for energy spreading. This additional correction results in nearly a factor of 2 increase for our highest energy point. It is generally less than a 25% increase for the bulk of the data. These efficiencies and the corresponding galactic fluxes are given in Table 3. The galactic e^- fluxes in the last column are

$$J_G = N_e/(A\Omega\tau\epsilon\Delta E_p\epsilon_p) .$$

Figure 5 shows the data transformed into galactic space, together with results of other experiments. The flux ratio $e^+/(e^+ + e^-)$ is reported to be ~ 0.1 (Buffington, Orth, and Smoot 1975; Golden *et al.* 1979*b*). Consequently, in Figure 5 the data for this experiment have been multiplied by 1.1 to correct for the fact that e^+ (which have positive curvature) were not included in the results in Table 3 but are not distinguished from e^- by most observers.

In order to fit the observations to a power-law spectrum, an absolute galactic e^- flux was computed, based on the choice of a normalization and spectral index. The assumed spectrum was then transformed into expected counts versus rigidity at the payload using the Monte Carlo program. This process was performed repetitively to obtain the best fit. Although the results are not very sensitive to solar modulation, a solar modulation of $\phi = 300$ MeV was assumed. The best values of the normalization and γ were obtained. The number of Monte Carlo cases was sufficient to ensure that uncertainties due to fluctuations in the calculation were negligible. The resulting flux is

$$J(E) = 367E^{-(3.15\pm0.20)}\ e^-\ m^{-2}\ sr^{-1}\ s^{-1}\ GeV^{-1} .$$

The uncertainty in the overall normalization is 10% and is dominated by uncertainty in the MWPC efficiency. The energy interval covered by the data is 4.5–62.5 GeV. The fit has a confidence level of 95%.

If the spectral index is constrained to be -3.0, the best fit has the form $J(E) = 273E^{-3.0}\ e^-\ m^{-2}\ sr^{-1}\ s^{-1}\ GeV^{-1}$ and a confidence level of 53%. These fits were obtained using a solar modulation value of 300 MeV, and a geomagnetic transmission function derived from the proton and alpha-particle fluxes observed during the same flight.

V. VALIDATION OF ABSOLUTE RATES

In this section, independent rate measurements are presented as yet another method for validating absolute rates measured with the magnet spectrometer system.

Table 4 shows a comparison of e^- absolute rates measured with different selection criteria and a more recent balloon flight. The data in the first row were selected using the same selection criteria as in Table 1 of this paper. The data in the second row were selected by the same criteria, except that no test of the G counter was made. This introduces a background from $\bar{p}$ and atmospheric mesons. Most of this additional background should be removed by the shower-counter background subtraction technique. Data in the third row were selected using the basic criteria of Table 1, but in addition all MWPC readouts were required to have good time sums and the trajectory fits had to have $\chi_x^2 < 30$, $\chi_y^2 < 8$. The imposition of very strict MWPC selection criteria tests the methodology of determining the MWPC efficiency, and also reduces the probability of background events due to multiple particles or other spu-

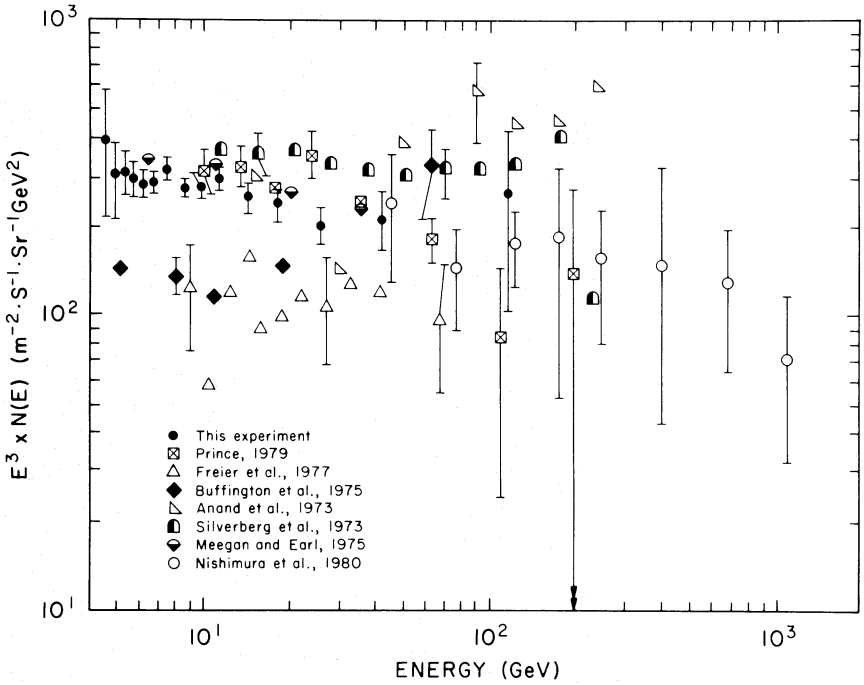

FIG. 5*a*

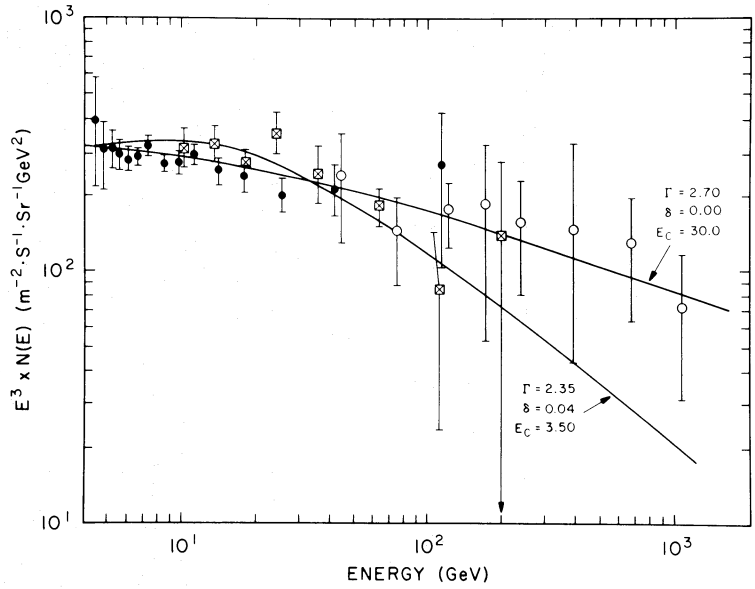

FIG. 5*b*

FIG. 5.—The electron data transformed to the interstellar medium. Figure 5*a* shows the data along with previously reported data. Since the other experiments were measurements of the total electron and positron flux, the authors' data have been multiplied by 1.1 for comparison. Figure 5*b* shows several leaky-box model predictions for the electron spectra. The two cases are for storage times $\tau \propto E^{-\delta}$, where $\delta = 0.0$ or 0.4. The energy at which radiant energy losses dominate escape losses (E_c) was adjusted for best fit in each case. The data from the two most recent observations at energies >100 GeV have also been plotted to illustrate the consistency among recent experiments.

rious trajectory measurements. The data in the fourth row are from another balloon flight. They represent a test of the sensitivity of the results to payload calibration and overall repeatability. Note that the Cerenkov efficiency was considerably higher for the data in the fourth row. This resulted from the use of gas with a higher index of refraction. The consistency of the four analyses is consistent with the estimated upper limit of 10% error in the absolute rates.

The absolute fluxes of protons, alpha-particles, sea-level muons, and atmospheric mesons have been measured as an additional consistency check. The available observations are presented in Table 5. Only experiments that incorporated measurement of each individual particle's energy have been included. Unfortunately, because of the paucity of observations it is difficult to draw any strong conclusions. Inclusion of results based on integral flux measurements does not clarify the

TABLE 4

ELECTRON RATES FOR DIFFERENT SELECTION CRITERIA

Description	Time (s)	Geometry Factor (cm^2 sr^{-1})	MWPC Efficiency	Energy-dependent Shower Efficiency	Charge Determination Efficiency	Cerenkov Detector Efficiency	Live-Time Fraction	$A\Omega\tau\epsilon$ (m^2 sr s)	Events above 8.33 GV/c (less Background)	Integral Flux (m sr^{-1} s^{-1})
G-on electron candidates	6.81×10^4	324	0.58	0.89	0.98	0.66	0.80	589	610	1.03 ± 0.09
Electron candidates without G test	6.81×10^4	324	0.58	0.89	0.98	1.00	0.80	892	1043	1.17 ± 0.10
G-on electrons with strict MWPC test	6.81×10^4	324	0.33	0.89	0.98	0.66	0.80	335	414	1.23 ± 0.12
G-on electron candidates from 1979 flight	2.84×10^4	256	0.58	0.89	0.98	0.93	0.87	297	302	1.01 ± 0.10

TABLE 5

INTEGRAL FLUXES ABOVE 10 GV/c

Reference	Type of Particle	Flux (No. of particles) m^{-2} sr^{-1} s^{-1}
This work	e^-	0.78 ± 0.08
This work	alpha	45 ± 5
Ryan, Ormes, and Balasubrahmangan 1972[a]	alpha	39 ± 8
Smith *et al.* 1973	alpha	25 ± 3
This work	proton	268 ± 27
Ryan, Ormes, and Balasubrahmanyan 1972[a]	proton	239 ± 24
Smith *et al.* 1973	proton	129 ± 19
This work	sea-level muon	1.03×10^{-3}
Allkofer, Carstensen, and Dau 1971[b]	sea-level muon	9.40×10^{-4}
This work	$(\mu^- + \pi^-)$ at altitude	1.0 ± 0.1
Stephens 1981[c]	$(\mu^- + \pi^-)$ at altitude	0.8 ± 0.1

[a] Flux values obtained by extrapolation based on a power law in kinetic energy. Extrapolation using a power law in rigidity results in a 13% lower flux for protons and 26% lower flux for alpha-particles.

[c] This is a result which is the midrange of a number of experiments. The experiments agree to within 10%. See Ayre *et al.* 1975 for additional data and results.

[b] The flux value was computed by Stephens 1981, using the inclusive reaction cross sections for meson production. This comparison was included because it constitutes a cross check for changes in muon detection efficiencies from those measured on the ground.

situation because they are no more consistent than the data in Table 5.

VI. DISCUSSION

Figure 5*a* shows that there has been considerable discrepancy in past observations of electrons. One explanation was that the observations with higher flux values were observations that suffered contamination due to protons. Figures 2–4 and Table 1 show by three independent means that the sample of electron candidates does not contain significant proton contamination below 25 GV/c. The cross-checks mentioned in the previous section lend additional credence to the absolute e^- rates derived in Table 3. The resulting absolute fluxes agree with the previous group of higher flux observations. The agreement implies that the previous high flux measurements are not contaminated by protons. It also implies that the low flux measurements are invalid. The low flux values could possibly be due to overestimation of the electron detection exposure factor.

Silverberg and Ramaty (1973) provide a discussion of various factors influencing the e^- energy spectrum. In general, the free parameters involved are the injection spectral index Γ, the energy dependence of the storage time δ [where $\tau(\text{storage}) = \tau_0 E^{-\delta}$], and the energy E_c at which the radiative loss lifetime equals the storage lifetime. The sum $\Gamma + \delta$ is thought to be about 2.75 (the observed proton spectral index). The data from Table 3 have been fitted for two cases, using the formulas of Silverberg and Ramaty (1973) for the predicted e^- spectrum. For $\Gamma = 2.75$, $\delta = 0$, we find $E_c = 30 \pm 7$ GeV, with a confidence level of 90% for the best fit. If we take $\Gamma = 2.25$ and $\delta = 0.4$, we find $E_c = 3.5 \pm 2$ GeV with a confidence level of 90%. The fits are shown in Figure 5*b*.

The values of E_c obtained from these fits can be related to the rms magnetic field traversed by the electrons during their storage (Silverberg and Ramaty 1973):

$$E_c = \frac{10^{16}}{[(3/16\pi)H_T^2 + W_{\rm ph}]\tau_0}\ (\text{GeV})\ ,$$

where H_T = rms transverse magnetic field (gauss); $W_{\rm ph}$ = average photon energy density in the interstellar medium (eV cm^{-3}); and τ_0 = storage lifetime of 1 GeV electrons (s).

Assuming $W_{\rm ph} = 0.7$ eV cm^{-3} and $\tau_0 = 10^7$ years, the values $E_c = 30$ and 3.5 GeV correspond to $H_T = 2.5$ and 12 microgauss, respectively. These values are generally associated with average galactic disk and denser cloud regions in the Galaxy. Unfortunately, to establish a precise value for H_T, the e^- spectrum would have to be measured to higher energies with greater precision.

VII. CONCLUSIONS

The results presented here offer a carefully validated observation of the e^- flux. It is in substantial agreement with observations of Prince (1979), Silverberg, Ormes, and Balasubrahmanyan (1973), Meegan and Earl (1975), and Nishimura *et al.* (1980). The observation disagrees with those of Buffington, Orth, and Smoot (1975) and Freier, Gilman and Waddington (1977). The observed flux is consistent with predicted spectra, assuming a power-law injection followed by radiative energy losses corresponding to a critical energy of $3 \lesssim E_c \lesssim 30$ GeV. Exact determination of the critical energy will require an observation with greater statistical accuracy, extending to energies well above 65 GeV. The data are also consistent with a simple power law in energy with a spectral index of 3.15 ± 0.2.

During the initial phases, this work was performed at the National Aeronautics and Space Administration's Johnson Space Center. The Lockheed Electronics Corporation acted as principal subcontractor at the Johnson Space Center. Since the relocation of the group to New Mexico State University (NMSU), NASA has supported the work through contract NAS9-15660 and grant NAGW-110. The staff at the Physical Science Laboratory of NMSU provided the expertise required to perform the experiment. Special thanks are due to the National Scientific Balloon Facility, which provided balloon flight support services at Palestine, Texas, and to P. Freier and W. R. Webber, who provided helpful comments and suggestions during the preparation of this paper.

REFERENCES

Allkofer, O. C., Carstensen, K., and Dau, W. D. 1971, *Proc. 12th Internat. Cosmic Ray Conf.* (Hobart), **4**, 1314.
Anand, K. C., Daniel, R. R., and Stephens, S. A. 1973, *Proc. 13th Internat. Cosmic Ray Conf.* (Denver), **1**, 355.
Ayre, C. A., Baxendale, J. M., Hume, C. J., Nandi, B. C., Thompson, M. G., and Whalley, M. R. 1975, *J. Phys. G*, **1**, 584.
Buffington, A., Orth, C. D., and Smoot, G. F. 1975, *Ap. J.*, **199**, 669.
Freier, P., Gilman, C., and Waddington, C. J. 1977, *Ap. J.*, **213**, 588.
Golden, R. L., Badhwar, G. D., Lacy, J. L., and Zipse, J. E. 1978, *Nucl. Instr. Meth.*, **148**, 179.
Golden, R. L., Horan, S., Mauger, B. G., Badhwar, G. D., Lacy, J. L., Stephens, S. A., Daniel, R. R., and Zipse, J. E. 1979*a*, *Phys. Rev. Letters*, **43**, 1196.
Golden, R. L., Lacy, J. L., Stephens, S. A., and Daniel, R. R. 1979*b*, *Proc. 16th Internat. Cosmic Ray Conf.* (Kyoto), **1**, 470.
Lacy, J. L., and Lindsey, R. S. 1974, *Nucl. Instr. Meth.*, **119**, 483.
Mauger, B. G. 1981, Ph.D. thesis, New Mexico State University.
Meegan, C. A., and Earl, J. A. 1975, *Ap. J.*, **197**, 219.
Nishimura, J., *et al.* 1980, *Ap. J.*, **238**, 394.
Prince, T. A. 1979, *Ap. J.*, **227**, 676.
Ryan, M. J., Ormes, J. F., and Balasubrahmanyan, V. K. 1972, *Phys. Rev. Letters*, **28**, 985; Erratum, *Phys. Rev. Letters*, **28**, 1497.
Silverberg, R. F., Ormes, J. F., and Balasubrahmanyan, V. K. 1973, *Proc. 13th Internat. Cosmic Ray Conf.* (Denver), **1**, 347.
Silverberg, R. F., and Ramaty, R. 1973, *Nature*, **243**, 134.
Smith, L. H., Buffington, A., Smoot, G. F., Alvarez, L. W., and Wahlig, M. A. 1973, *Ap. J.*, **180**, 987.
Stephens, S. A. 1981, *Proc. 17th Internat. Cosmic Ray Conf.* (Paris), **4**, 282.

G. D. BADHWAR and J. L. LACY: NASA/Johnson Space Center, Houston, TX 77058

R. R. DANIEL and S. A. STEPHENS: Tata Institute of Fundamental Research, Homi Bhabda Road, Bombay, India 400-005

R. L. GOLDEN: EE Department, P.O. Box 30, Las Cruces, NM 88003

B. G. MAUGER: Spacecom Inc., P.O. Box 235, Las Cruces, NM 88004

J. E. ZIPSE: Jet Propulsion Laboratory, Pasadena, CA 91103